



SKIM-MPRC TN-6: Remote Sensing Spatial Simulator (R3S)



(Deliverable SWB1)

Submitted by:



LOPS, France

Customer	ESA
Author	LOPS
ESA ITT Number	4000124664/18/NL/NA
Document Reference	SKIM-MPRC_LOPS_2019
SoW Reference	ESA-EOPSM-SKIM-SOW-3262
Version/Revision	1.0
Date of issue	April 30, 2019

Issued by (LOPS)	Frederic Nouguier	2019/04/30	
Reviewed by (LOPS)	Bertrand Chapron	2019/04/30	
Approved by (ESA)	Craig Donlon	Date and signature	

Chronology			
Issue	Date	Change record	Author
0.1	2019/04/15	Initial document	F. Nouguier
1.0	2019/04/30	Finalized and delivered	F. Nouguier

Contents

1	Introduction	5
1.1	Wave Doppler signal	5
1.2	Simulation	5
2	Ocean scene simulation and facets decomposition	6
2.1	A Fourier Transform Ocean surface	6
2.2	Numerical implementation	6
2.3	Facet decomposition	7
3	Scattering calculation in SKIM geometry	8
3.1	Rolling the ocean surface under the beam footprint	8
3.2	Updating surface geometry.	8
3.3	Electromagnetic contribution of facets.	8
3.3.1	Normalized Radar Cross Section and Doppler pulsation of facets	9
3.4	Facet’s registration	9
4	On Board Processing (OBP)	11
4.1	PTR and range compression	11
4.2	Slant to ground projection	11
4.3	Migration	12
4.4	Normalized Radar Cross Section, pulse pair and modulations	12
4.4.1	NRCS	12
4.4.1.1	Regular ground gate interpolation:	13
4.4.2	Doppler modulations	13
4.4.3	Mean Doppler shift	14
4.4.4	Additional remark	14

5	Post-processing	15
5.1	Platform velocity Doppler	15
5.2	NRCS spectrum	15
5.3	Pulse pair phase spectrum	16
5.4	Mean Geophysical Doppler	16
6	Numerical implementation	19
6.1	Code language	19
6.2	Input parameters	19
6.3	Output files	21
6.4	Flow diagram	21
6.5	Numerical code	21
A	Appendix subsection	21
	Bibliography	21

1 Introduction

From SKIM measurements, the dynamical properties of the ocean surface are extracted from the correlation properties of both the back-scatter complex field and its associated intensity. The sea surface roughness is characterized by a very broad scale distribution, from $O(1\text{mm})$ to $O(100\text{ m})$, having distinct spatio-temporal correlation lengths. It leads to highly fluctuating instantaneous back-scattered intensities, the radar sea clutter. The latter then takes the form of a multiplicative random processes, separating fluctuation contributions between different ocean surface scales.

1.1 Wave Doppler signal

From the averaged time-correlation measurements, SKaR sensor will provide Doppler measurements in looking direction. As mentioned above, this Doppler integrates several components that have to be isolated in order to be able to recover the contribution of the ocean surface current projected on the radial direction. The main identified components that can sign on the measured Doppler can be divided in a non-geophysical part coming from the platform velocity, a geophysical part due to ocean (waves and current) kinematics and a cross-component coming from a geophysical weighting of the platform velocity.

From a radar-ocean measurement perspective, it is understood that the measured time-varying intensities cannot be exactly predicted in advance, even though the macroscopic statistical properties of the moving rough ocean surface would be exactly known. Rather, we can only predict some overall statistical properties of the time-varying intensities over an ensemble of rough surfaces. In the context of SKaR, high-frequency near-nadir measurements, a Kirchhoff-Approximation (KA) can be used, and it has been identified (Nouguier et al. (2018)) that, on the mean, the overall scatter velocity largely dominates the total geophysical Doppler, to be as high as 50 times the Stokes drift velocity.

To help understand how the SKaR sensor is able to provide meaningful statistical information, i.e. directional wave and motion properties, and to further define a retrieval strategy to isolate these contributions from the geophysical Doppler signal, a numerical simulator has been defined. Operating at very high-frequency, fast fluctuations associated with short-scale ripples can be distinguished from longer modulating scales. Typically, longer scales correspond to ocean waves larger than short scale rough facets. As such, we can estimate any average quantity, first with respect to the faster varying scales, and then to with respect to the longer components. Numerically, these longer wave components will be resolved, and the short-scale rough and fast varying components will be prescribed, statistically constrained.

1.2 Simulation

The purpose of this document is to present the chosen methodology for the simulation of SKIM data at PRF rate (RAW signals). It describes how On-Board-Processing methods (range compression, migration, averaging, NRCS, pulse-pair ...) are taken into account and applied to RAW signals (LO data). It also presents the technique applied to compute NRCS and Pulse-Pair modulation spectra and useful methods to derive wave spectrum that is the main input parameter used for Wave Doppler estimation.

This document is divided in four sections.

- Ocean scene simulation and facets decomposition
- Scattering calculation in SKIM geometry
- On Board Processing
- Post-processing
- Numerical implementation

2 Ocean scene simulation and facets decomposition

2.1 A Fourier Transform Ocean surface

In this section, we focus on how ocean surface waves are generated. The sea surface scene generation is the numerical evaluation of the sea surface profile over a user-defined region. A linear surface profile is a superposition of independent harmonic waves travelling with their associated wave linear dispersion. The geophysical entry of such a model is the directional sea surface spectrum : $S_d(\mathbf{k})$ where \mathbf{k} is the directional spatial wave-vector

$$\mathbf{k} = \frac{2\pi}{\lambda} \hat{\mathbf{k}} \quad (1)$$

with $\lambda = \frac{2\pi}{k}$ the sine wavelength and $\hat{\mathbf{k}} = \frac{\mathbf{k}}{k}$ the wave direction.

A realization of a linear random surface elevation η writes **nouguier2009**

$$\eta(\mathbf{r}, t) = \int_{\mathbb{R}^2} d\mathbf{k} a(\mathbf{k}) e^{i(\mathbf{k} \cdot \mathbf{r} - \omega t)} + c.c. \quad (2)$$

where t is the time, $\mathbf{r} = (x, y)$ is the horizontal location, $a(\mathbf{k})$ is half the complex wave amplitude of wave \mathbf{k} with random phase in $[0, 2\pi[$ and $c.c.$ is the complex conjugate.

$$\omega = \sqrt{gk} \quad \text{is the linear relation ship without current.} \quad (3)$$

$$\omega = \sqrt{gk} + \mathbf{k} \cdot \mathbf{U} \quad \text{is the linear relation ship with a current } \mathbf{U}. \quad (4)$$

It rewrites:

$$\eta(\mathbf{r}, t) = \int_{\mathbb{R}^2} d\mathbf{k} [a(\mathbf{k}) e^{-i\omega t} + a^*(-\mathbf{k}) e^{i\omega t}] e^{i\mathbf{k} \cdot \mathbf{r}} \quad (5)$$

Assuming that η is a stationary process, the elevation cross-correlation $\rho(\mathbf{r} - \mathbf{r}', t - t') = \langle \eta(\mathbf{r}, t) \eta(\mathbf{r}', t') \rangle$ writes:

$$\rho(\boldsymbol{\xi}, \tau) = \int_{\mathbb{R}^2} d\mathbf{k} [S_d(\mathbf{k}) e^{-i\omega\tau} + S_d^*(-\mathbf{k}) e^{i\omega\tau}] e^{i\mathbf{k} \cdot \boldsymbol{\xi}} \quad (6)$$

where $S_d(\mathbf{k})$ is defined by

$$\langle a(\mathbf{k}) a^*(\mathbf{k}') \rangle = S_d(\mathbf{k}) \delta(\mathbf{k} - \mathbf{k}') \quad (7)$$

and where the brackets stand for statistical averaging.

$S_d(\mathbf{k})$ is half the square amplitude of wave \mathbf{k} and is real. S_d is the directive oceanic spectrum which is not centro-symmetric. It follows that:

$$S(\mathbf{k}) = S_d(\mathbf{k}) + S_d(-\mathbf{k}) \quad (8)$$

is the well known centro-symmetric spectrum.

2.2 Numerical implementation

A surface spectrum $S_d(\mathbf{k})$ is provided by the user or evaluated according to prescribed equations (Elfouhaily et al.).

$S_d(\mathbf{k})$ is evaluated over a regular wave-number Cartesian grid (k_x, k_y) . The grid over which the spectrum is evaluated depends on the user requirements such as surface width (L_x, L_y) and spatial sampling (d_x, d_y) . The spectrum is naturally truncated at $k_{min} = \left(\frac{2\pi}{L_x}, \frac{2\pi}{L_y}\right)$ and $k_{max} = \left(\frac{2\pi}{2d_x}, \frac{2\pi}{2d_y}\right)$ in order to respect Shannon Theorem.

For a given time, evaluation of equation (2) is numerically realized with an FFT algorithm. This implies the surface to be periodic. An example of surface is given on figure 1

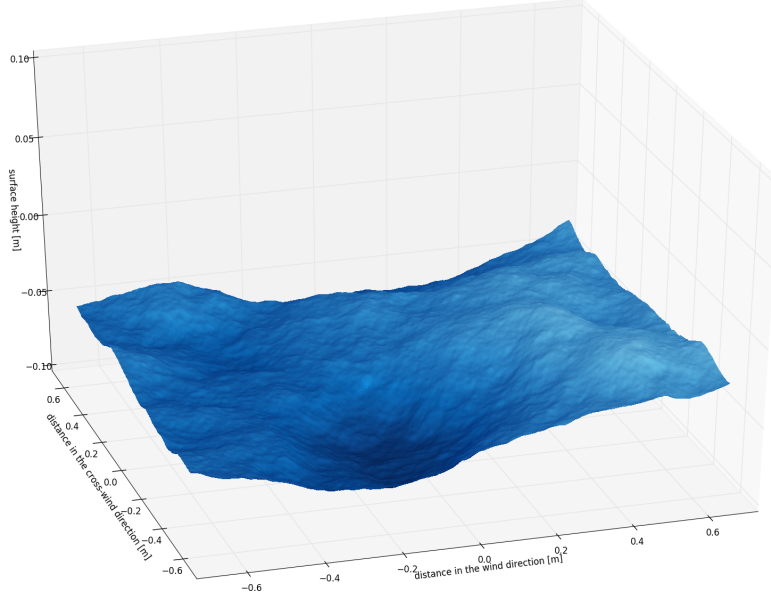


Figure 1: Extraction of a $1.3 \text{ m} \times 1.3 \text{ m}$ patch of a larger surface scene.

2.3 Facet decomposition

The ocean surface profile is given over a spatial grid and elevation points are noted by their 3 dimensional coordinates $\mathbf{P}_{i,j} = (x_{i,j}, y_{i,j}, z_{i,j})$, where “i” and “j” refers to “x” and “y” directions.

An “upper” and “lower” triangular facets are respectively defined by their centroid coordinates:

$$\mathbf{C}_{i,j}^u = \frac{\mathbf{P}_{i,j} + \mathbf{P}_{i+1,j} + \mathbf{P}_{i,j+1}}{3} \quad \text{and} \quad \mathbf{C}_{i,j}^l = \frac{\mathbf{P}_{i+1,j+1} + \mathbf{P}_{i+1,j} + \mathbf{P}_{i,j+1}}{3} \quad (9)$$

The facets normal vector are defined by:

$$\mathbf{n}_{i,j}^u = (\mathbf{R}_{i+1,j} - \mathbf{R}_{i,j}) \times (\mathbf{R}_{i,j+1} - \mathbf{R}_{i,j}) \quad \text{and} \quad \mathbf{n}_{i,j}^l = (\mathbf{R}_{i,j+1} - \mathbf{R}_{i+1,j+1}) \times (\mathbf{R}_{i+1,j} - \mathbf{R}_{i+1,j+1}) \quad (10)$$

where \times is the cross product. The normalized normal vector $\hat{\mathbf{n}}_{i,j}^{u,l}$ and the triangular facet areas $a_{i,j}^{u,l}$ correspond to the directions and the norms of vectors in equation (10), respectively.

3 Scattering calculation in SKIM geometry

3.1 Rolling the ocean surface under the beam footprint

Numerical evaluation of equation (2) provide a numerical surface profile of size (L_x, L_y) and spatial sampling (d_x, d_y) but it can be considered as infinite in space due to periodic characteristic of FFT algorithm. Prohibitive numerical costs hampers the generation of a surface as large as the satellite swath (> 100 km) with the required meaningful spatial sampling (≈ 1 meter). However, a surface as large as the beam footprint ($\approx 20\text{km} \times 20\text{km}$) is largely tractable. The surface has then to be generated under the footprint.

For a numerical point of view, surface generation and scattering calculation are asynchronous. It means that at the moment the surface is numerically evaluated, the footprint position is not absolutely defined. At each emitted pulse, the surface is thus rolled (not translated) under the beam footprint.

3.2 Updating surface geometry.

Due to the very high Pulse Repetition Frequency (PRF) of the instrument, it would be too numerically demanding to update the surface elevation profile at each pulse. Moreover, typical time scale of the surface evolution is much longer (≈ 1 milliseconds) than the PRI ($\approx 36\mu\text{second}$). It is thus only relevant to update the surface at a slower time rate, corresponding to the appropriate surface evolution.

Nevertheless, surface evolution has to be taken into account for each PRI time step. This is achieved by interpolating the surface profiles between two surface time steps. At each instrument pulse, the two closest surface time steps are found and the facets geometry (centroids, areas and normal vectors) is interpolated according to the pulse time.

3.3 Electromagnetic contribution of facets.

The contribution of a surface facet labeled with (i, j) pair writes:

$$E_{i,j} = \frac{1}{R_{i,j}^2} \sqrt{G_{i,j} a_{i,j} \sigma_{i,j}^0} e^{i(2\mathbf{K} \cdot \mathbf{R}_{i,j} + i\omega_{D_{i,j}} t + \phi_{i,j})} \quad (11)$$

where we have:

- $G_{i,j}$: Two way power antenna Gain in the satellite to facet direction
- \mathbf{K} : Electromagnetic wavevector of norm $2\pi/\lambda_{em}$
- $a_{i,j}$: Area of the facet
- $R_{i,j}$: Distance between facet and satellite antenna
- $\sigma_{i,j}^0$: Normalized Radar Cross Section for a given facet (see section 3.3.1)
- $\omega_{D_{i,j}}$: Doppler pulsation of the facet (see section 3.3.1)
- $\phi_{i,j}$: Random phase of the facet

$\phi_{i,j}$ is a random phase whose spatio-temporal distribution will control the overall speckle characteristics. As a first assumption, we assume that, each facet phase is uncorrelated with other facets ones. We moreover assume that the life-time of facet scatters is large compared to the cycle duration. Consequently, $\phi_{i,j}$ is a random variable with uniform distribution over $[0, 2\pi[$ domain, but is kept constant over an instrument cycle.

3.3.1 Normalized Radar Cross Section and Doppler pulsation of facets

Due to a limited spatial sampling of the surface, a Normalized Radar Cross Section (NRCS) and a doppler pulsation for each facet has to be prescribed. To do so, we rely on classical asymptotic methods whose validity domain has been well established. The numerical implementation enables full flexibility to change which asymptotic method is used. In the SKIM configuration (Ka-band and near nadir incidence angles), the Physical Optics / Kirchhoff approximation KA is considered (Nouguier et al. (2016); Nouguier et al. (2018)).

The KA define the NRCS as:

$$\sigma^0 = \frac{1}{\pi} \frac{|\mathcal{K}|^2}{(2K)^2} \sec^2(\theta) \zeta^0, \quad (12)$$

and the Doppler pulsation (Mouche et al. (2005); Nouguier et al. (2018)) as

$$\omega_D = -i\partial_\tau \zeta^0 / \zeta^0 \quad (13)$$

with

$$\zeta(\tau) = \int_A e^{i\mathbf{Q}_H \cdot \boldsymbol{\xi}} e^{-Q_z^2(\rho(0,0) - \rho(\boldsymbol{\xi}, \tau))} d\boldsymbol{\xi}. \quad (14)$$

and where superscript ⁰ stands for an average taken at $\tau = 0$. We have denoted \mathbf{K}_0 and \mathbf{K} , the incident and scattered EM wave vectors, with their respective horizontal \mathbf{k}_0 , \mathbf{k} and vertical $-q_0$, q components, one has

$$\mathbf{K}_0 = \mathbf{k}_0 - q_0 \hat{\mathbf{z}}, \quad \mathbf{K} = \mathbf{k} + q \hat{\mathbf{z}}, \quad (15)$$

with positive q and q_0 given by $k_0^2 + q_0^2 = k^2 + q^2 = K_0^2$. The Ewald vector is defined as $\mathbf{Q} = \mathbf{K} - \mathbf{K}_0$ with horizontal $\mathbf{Q}_H = \mathbf{k} - \mathbf{k}_0$ and vertical $Q_z = q + q_0$ components. The ρ function is the spatio-temporal surface elevation correlation function, whose expression follows equation (6). The ‘‘unresolved wave spectrum’’, aka the wave directional energy spectrum of waves smaller than the surface spatial resolution, is further assumed to be defined using the Elfouhaily spectrum (Elfouhaily et al. (1997)). Note, all these quantities are azimuth dependent.

In the simulation, equation (12) has to be evaluated for each facet where the incidence angle (θ) is the local incidence ie, the angle between the local incident electromagnetic vector and the facet normal.

Numerically, the unresolved spectrum and unresolved correlation function are computed only once. The corresponding σ^0 (equation (12)) is computed for all possible incidence and azimuth angles and results are stored. For each facet, the local incidence and azimuth are evaluated and the corresponding NRCS is found by interpolation. Figure (2) and (3) show the NRCS and Doppler versus incidence and azimuth angles for a fully developed 7 m/s wind speed Elfouhaily spectrum.

3.4 Facet’s registration

In real measurement, range compression is acting to register facet contribution to the corresponding slant gate distance. In the current numerical code, synthetic signals are modeled after the range compression operation. Each facet contribution is thus directly affected to the corresponding slant gate depending on its distance to the antenna : $R_{i,j}$. The complex electromagnetic signal at slant range gate k and pulse p thus writes:

$$E^p(k) = \sum_{i,j} E_{i,j}^p \delta(|R_{i,j}^p - s_k| < \Delta s / 2) \quad (16)$$

where s_k is the slant distance at the middle of gate k and Δs is the slant resolution: $\Delta s = \frac{c}{2B}$ with c the speed of light and B the frequency bandwidth of the chirp. Real measurements correspond to the back-scatter electromagnetic signals (I and Q), as a function of time, and thus can directly be mapped as a function of slant gate distance (through a $2/c$ factor).

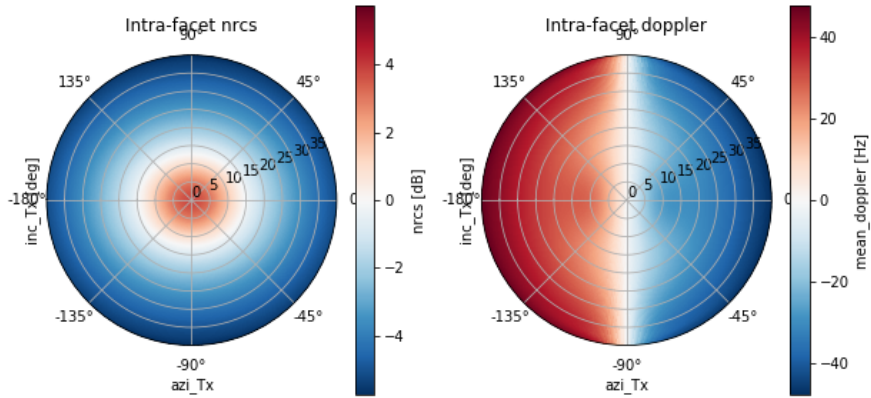


Figure 2: Example of NRCS and mean Doppler of facets for a fully developed 7 m/s wind speed Elfouhaily spectrum. Wind direction has been set to 0 deg.

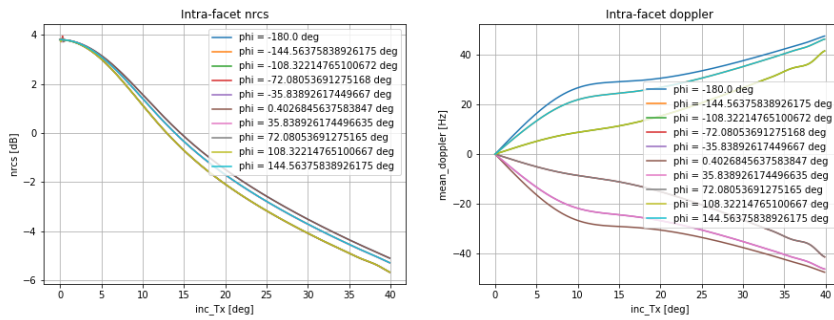


Figure 3: Azimuthal transects of figure 2.

4 On Board Processing (OBP)

4.1 PTR and range compression

In real OBP, both migration and range compression are applied through the chirp scaling operation. Compressed signals are thus convoluted by the chirp response in the physical space. To take this operation into account in the present simulations, synthetic signals $E(k) = I(k) + iQ(k)$ are re-sampled with an artificial high slant gate resolution (typically $\Delta s/10$), and further convoluted with the Point Target Response PTR of the range compression operation. The re-sampled signals are termed hereafter as "numerical signals". For our purpose, a sinc function is used in the simulation to simulate the PTR convolution:

$$PTR(k) = \frac{1.2}{\Delta s} \text{sinc} \left(\frac{1.2}{\Delta s} k \right) \tag{17}$$

4.2 Slant to ground projection

Ground gate positions are the distance between the ground projected position of the satellite and the ground position corresponding to a slant gate distance.

B\

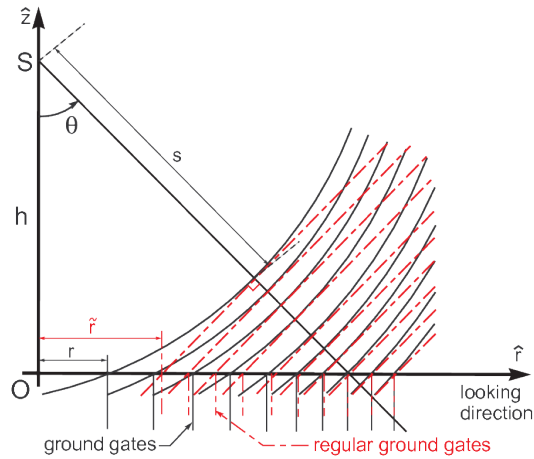


Figure 4: Slant to ground projection geometry.

It writes:

$$r = \sqrt{s^2 - h^2} \tag{18}$$

with

- r : ground range distance
- s : slant range distance
- h : satellite altitude

4.3 Migration

The migration is an OBP operation applied to compensate the motion of the satellite relative to the Earth surface. This operation has to be operated prior to pulse averaging operation in order to coherently accumulate signals from the same scatters. To minimize the motion of the satellite on the accumulation operation, pulses of the same cycle are migrated over a chosen "reference pulse", corresponding to the middle pulse of the cycle in the current SKIM baseline. In the chirp scaling operation, both Earth rotundity and rotation have to be compensated. However, in the current version of the numerical code, the Earth is assumed to be flat and is not rotating. We thus do not need to compensate for the Earth rotundity and speed under the satellite. The simulation implicitly assume that these two effects have already been perfectly compensated, and only the satellite motion has to be corrected. Moreover, for practical reasons in the current version of the code, the migration is applied on ground projected signals, whereas real OBP operations generally apply the chirp scaling on slant range signals.

Figure 5 represents the ground geometry where M is a point on the ground that have to be migrated. We note:

- O_{ref} : ground projected satellite position at the reference pulse
- O : ground projected satellite position at the pulse to migrate
- r' : ground range distance (migrated)
- r : ground range distance to migrate
- φ_{ref} : azimuth of the antenna at reference pulse. From along track direction, clockwise
- φ : azimuth of the antenna of pulse to migrate. From along track direction, clockwise
- d : distance travelled between the reference pulse and the pulse to migrate.

It easily comes:

$$r' = r \cos(\varphi - \varphi_{ref}) + d \cos(\varphi_{ref}) \quad (19)$$

4.4 Normalized Radar Cross Section, pulse pair and modulations

4.4.1 NRCS

To evaluate NRCS modulations, a normalization by the slant distance and the illuminated area is applied on each complex RAW signals $E^p(k) = I^p(k) + iQ^p(k)$:

$$\bar{E}^p(k) = \frac{R^2(k)E^p(k)}{\sqrt{\mathcal{A}(k)}} \quad (20)$$

where

- $R(k)$: Slant distance of slant gate k
- $E^p(k)$: RAW complex signal
- $\mathcal{A}(k)$: Illuminated area of gate k , weighted by the antenna gain pattern

The normalization by the weighted area $\mathcal{A}(k)$ is done on pulse averaged signals, and provided by the antenna manufacturer or realized during the Calibration/Validation period. In the current numerical code, it is numerically evaluated as:

$$\mathcal{A}(k) = \sum_{i,j} G_{i,j} a_{i,j} \delta(|R_{i,j}^p - s_k| < \Delta s/2) \quad (21)$$

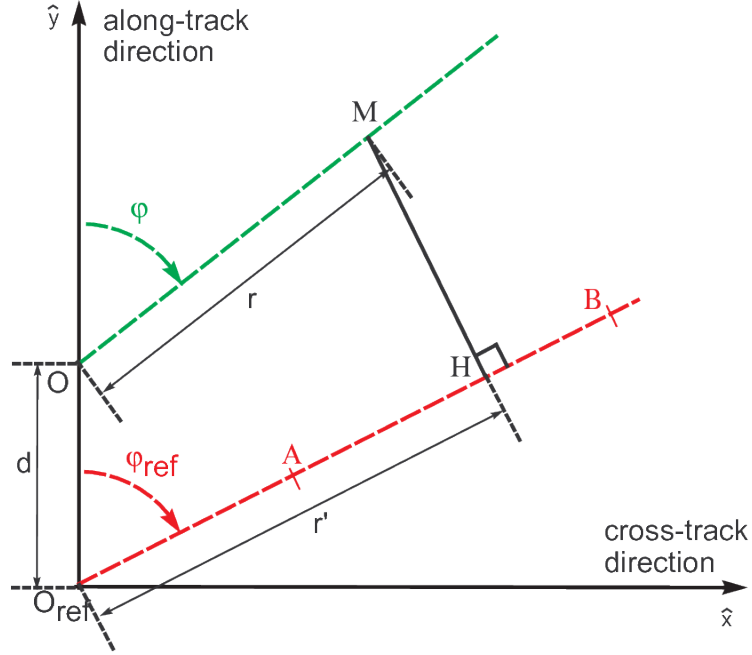


Figure 5: Range migration geometry.

where (i, j) are the facets of a flat surface. The normalization is applied for each pulse prior to pulse averaging.

4.4.1.1 Regular ground gate interpolation:

For practical reasons and spectral analysis of expected NRCS modulation, it is easier to work with a regular ground sampling. Thus, for numerical efficiency, “slant to ground projection”, “range migration” and “interpolation on a regular ground grid” are applied at the same time on normalized signals $\bar{E}^p(k)$ with an interpolation method.

The spatial sampling of the regular grid is set to:

$$\Delta\tilde{r} = \frac{\Delta s}{\sin\theta} \quad (22)$$

where θ is the fixed beam incidence ($\theta = 6$ or 12 deg). See figure 4 for geometry.

The output complex signal of these three operations is called “regular signal” and is a function of the regular ground gate distance \tilde{r} . We adopt the notation:

$$\tilde{E}^p(\tilde{r}) \quad (23)$$

The NRCS modulation profile easily comes as:

$$\tilde{\sigma}^0(\tilde{r}) = \langle \tilde{E}^p(\tilde{r}) \rangle_p \quad (24)$$

where $\langle \cdot \rangle_p$ means averaging over pulses

4.4.2 Doppler modulations

The averaged pulse pair product writes:

$$PP(\tilde{r}) = \langle \tilde{E}^p(\tilde{r}) \tilde{E}^{*p+1}(\tilde{r}) \rangle_p \quad (25)$$

and the Doppler modulations thus comes as:

$$\tilde{f}_D(\tilde{r}) = \frac{PRF}{2\pi} \text{Arg}[PP(\tilde{r})] \quad (26)$$

4.4.3 Mean Doppler shift

The mean Doppler frequency of the scene writes:

$$f_D = \frac{PRF}{2\pi} \text{Arg} \left[\langle \tilde{E}^p(\tilde{r}) \tilde{E}^{*p+1}(\tilde{r}) \rangle_{p, \tilde{r}} \right] \quad (27)$$

4.4.4 Additional remark

The normalization (20) between \bar{E}^p and \tilde{E}^p before any averaging is not realized in the actual OBP. This normalization can introduce small biases, in particular on the mean Doppler shift of the scene as the antenna pattern can slightly change the weight of the different gates in the range averaging. However, for our purpose, this normalization has been done prior to pulse and range averaging in order to more readily compare with the theory of Nougier et al. (2018). This normalization can also be done after all averaging and some verification of expected small biases could be done.

5 Post-processing

5.1 Platform velocity Doppler

Due to platform velocity, a Non-Geophysical (NG) Doppler shift is contained in (25). Taking immediately the argument of PP in (26) makes the phase turning more than 2π over range. Figure 6 shows an example of the phase of each pulse pair ($Arg [\tilde{E}^p(\tilde{r})E^{p+1}(\tilde{r})^*]$) as a function of range and pulse. We can clearly see the pulse and range trends of the phase.

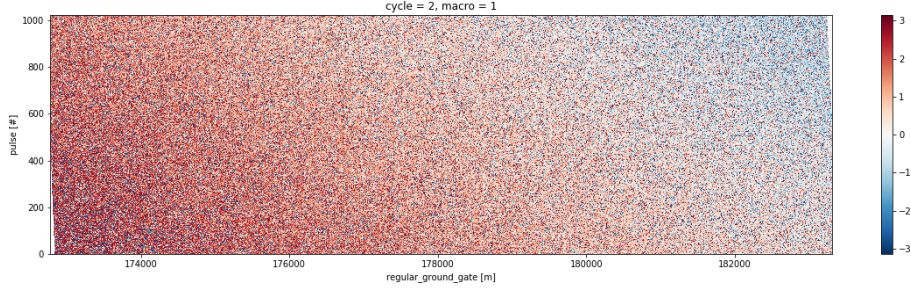


Figure 6: Example of phase of each pulse-pair [rad]. Antenna azimuth = 126 deg.

The platform velocity phase has to be removed from the pulse-pair product to ensure proper removal of the Non Geophysical Doppler. It writes:

$$\Phi^p(k) = 2\pi V_g \sin(\theta^p(k)) \cos(\varphi^p) PRF / c \quad (28)$$

where

- V_g : Satellite ground speed
- $\theta(k)$: Local EM vector incidence on a flat slant gate k
- φ^p : Antenna azimuth of pulse p

In the the current implementation of the numerical code, $e^{i\Phi^p(k)}$ is slant-to-ground projected, range-migrated and interpolated over the regular ground grid, (naming $e^{i\tilde{\Phi}^p(\tilde{r})}$) and then subtracted to the pulse-pair products phase to finally give the Geophysical Doppler frequency:

$$\tilde{f}_{GD}(\tilde{r}) = \frac{PRF}{2\pi} Arg \left[\left\langle \tilde{E}^p(\tilde{r}) \tilde{E}^{*p+1}(\tilde{r}) e^{-i\tilde{\Phi}^p(\tilde{r})} \right\rangle_p \right] \quad (29)$$

We can note that $\Phi^p(k)$ is solely geometry dependent and not related to the geophysical signals. In reality, this NG Doppler will thus be evaluated through platform attitude measurements and calibration and removed after pulse averaging.

Figure 7 shows the corrected phase ($Arg [\tilde{E}^p(\tilde{r}) \tilde{E}^{*p+1}(\tilde{r}) e^{-i\tilde{\Phi}^p(\tilde{r})}]$).

To recall, 6 and 7 are for illustration purpose only, and that the phase of the pulse pair product is taken after pulse averaging.

5.2 NRCS spectrum

For each cycle, a range profile of the normalized radar cross section is given through equation (24). The 1D NRCS periodogram

$$S_{\tilde{\sigma}^0}^{1D}(k) = \left\langle \left| \int e^{ik\tilde{r}} \tilde{\sigma}^0(\tilde{r}) d\tilde{r} \right|^2 \right\rangle \quad (30)$$

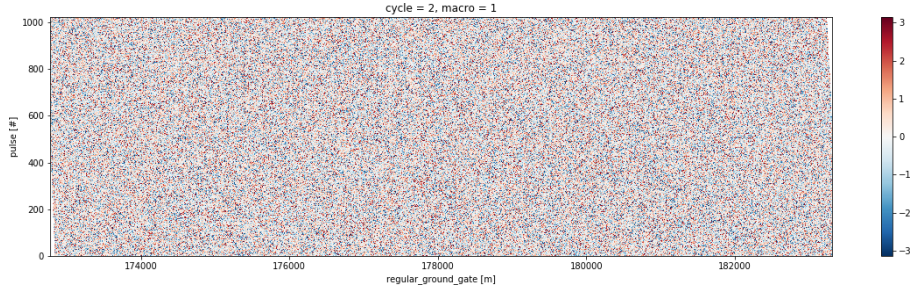


Figure 7: Corrected phase of each pulse-pair [rad]. Antenna azimuth = 126 deg.

where $\langle \cdot \rangle$ the average operation, is evaluated with a Welch standard method over a chosen number of range points and weighting window. Figure 8 and 9 show example of NRCS modulations and associated periodogram.

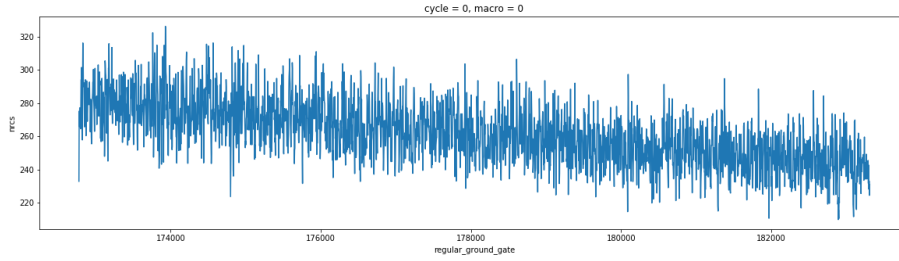


Figure 8: Example of NRCS modulations obtained at 12 degrees incidence.

Each 1D NRCS spectrum is a transect of the directional NRCS spectrum at the mean azimuth of the cycle. After a complete antenna rotation, we can thus define the directional σ^0 modulation spectrum:

$$S_{\sigma^0}(\mathbf{k}) = S_{\sigma^0}(k, \phi) \quad (31)$$

Figure 10 shows an example of a directional spectrum obtained after one antenna turn. We can see the wave signal coming/going in the +90/-90 degrees (cross-track) direction.

5.3 Pulse pair phase spectrum

For each cycle, a range profile of the modulated geophysical Doppler frequency is given through equation (29). The same methodology as for NRCS modulations (see section 5.2) is applied to $\tilde{f}_{GD}(\tilde{r})$:

$$S_{\tilde{f}_{GD}}^{1D}(k) = \left\langle \left| \int e^{ik\tilde{r}} \tilde{f}_{GD}(\tilde{r}) d\tilde{r} \right|^2 \right\rangle \quad (32)$$

giving access, after a complete antenna turn, to the directional Doppler frequency modulation spectrum: $S_{\tilde{f}_{GD}}(\mathbf{k})$.

5.4 Mean Geophysical Doppler

A mean Geophysical Doppler frequency of the ocean scene is define for each cycle as:

$$f_{GD} = \frac{PRF}{2\pi} \text{Arg} \left[\left\langle \tilde{E}^p(\tilde{r}) \tilde{E}^{*p+1}(\tilde{r}) e^{-i\Phi^p(\tilde{r})} \right\rangle_{p, \tilde{r}} \right] \quad (33)$$

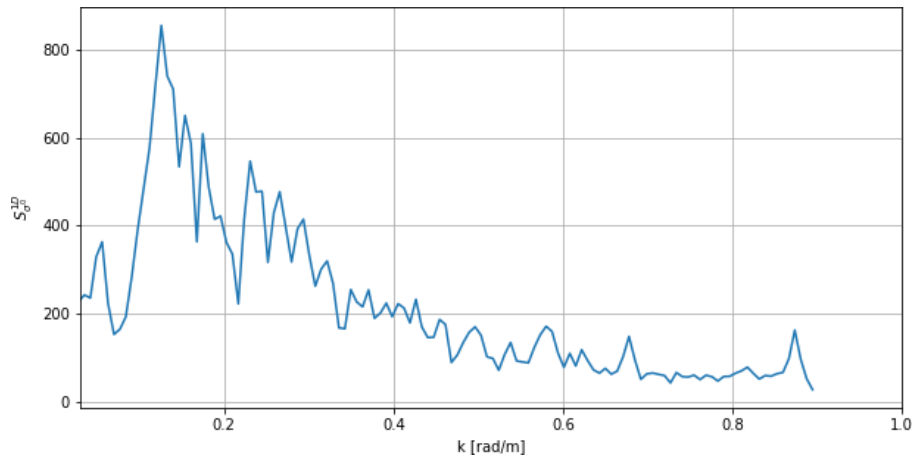


Figure 9: Periodogram of detrended signal shown figure 8.

Figure 11 shows an example of f_{GD} against antenna azimuth obtained after a complete antenna turn simulation with a 12 degrees incidence configuration. The ocean scene was simulated with a full developed Elfouhaily wind sea spectrum parametrized with a 7 m/s wind speed at 90 degrees from the uptrack (0 deg) direction. We can see the maximal geophysical contribution of the waves in the 90 ± 180 deg direction dominated by a strong peak at 235 ± 180 degrees coming from the cross-component of the geophysical weighting of the platform velocity.

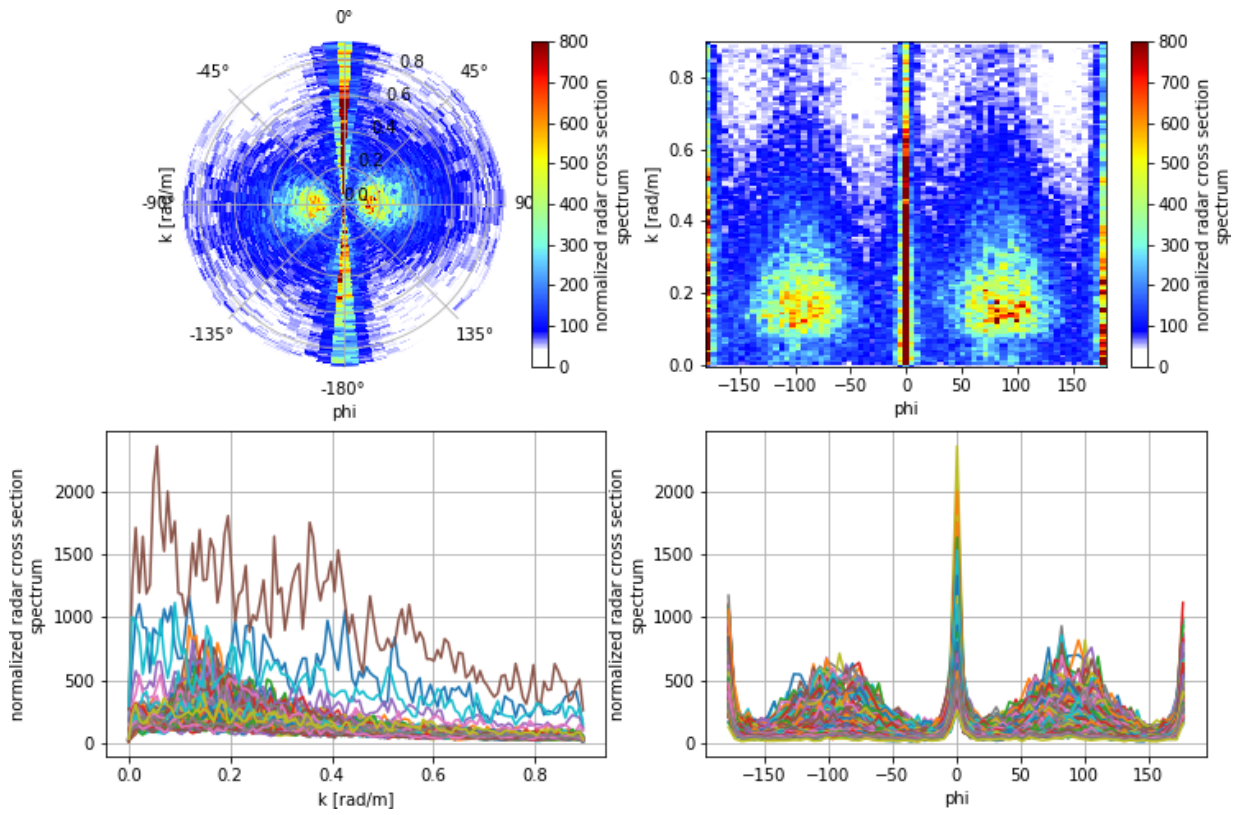


Figure 10: Directional representations of NRCS modulation spectrum obtained at 1 degrees incidence. From left to right and top to bottom: Polar and Cartesian representation. Transects in azimuth and wavenumber directions.

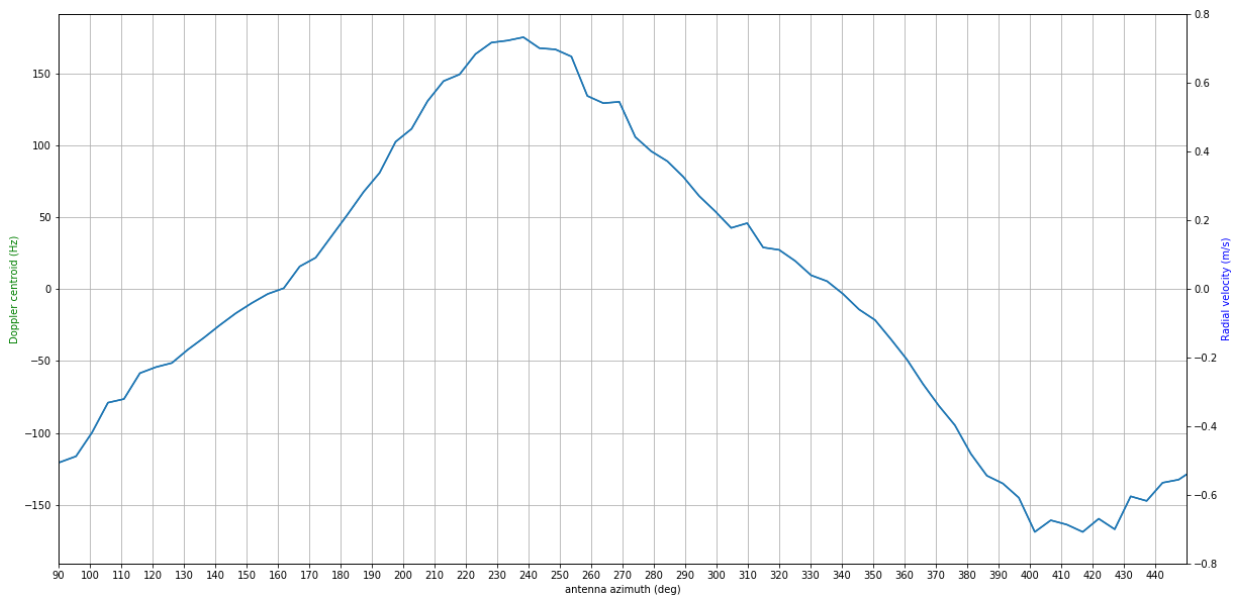


Figure 11: Mean geophysical Doppler frequency versus antenna azimuth obtained at 12 degrees incidence.

6 Numerical implementation

6.1 Code language

The numerical code has been entirely developed with the free and open language: python (3.6). Due to the very high PRF of the instrument and the needed fine resolution of the ocean scene, numerical computations have a high numerical cost. The use of High Performance Computer (HPC) is needed and we choose to rely on the growing *Open Source Big Data Climate Science Platform: Pangeo* (see figure 12). This platform is mainly divided in two important libraries: *dask* and *xarray* which respectively handle distributed calculation and easy manipulation of netcdf-like structures. Basic numerical calculations rely on *NumPy* library efficiency.

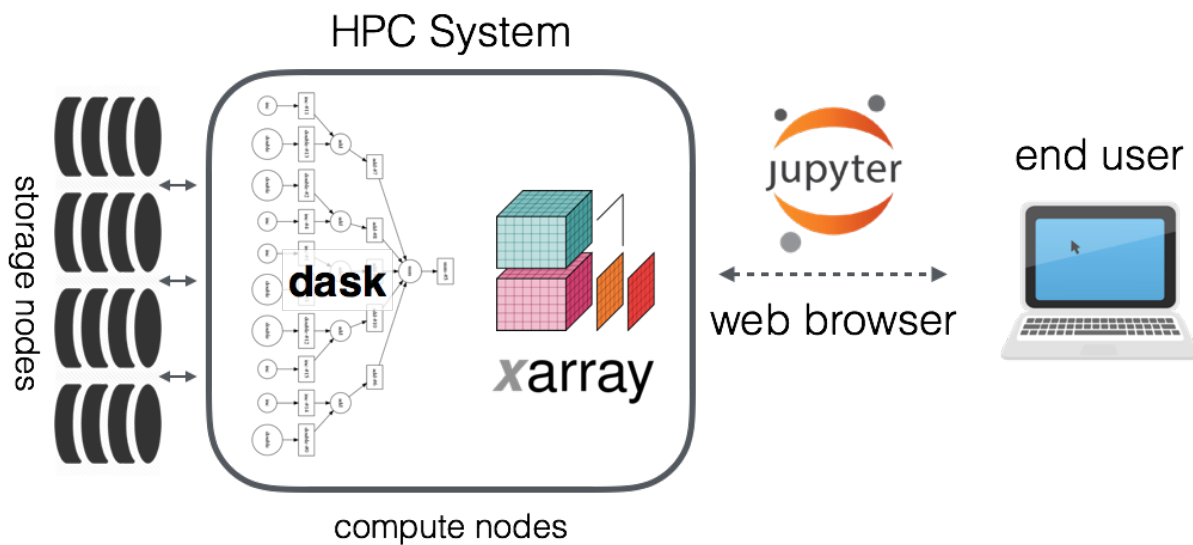


Figure 12: Caption: The Pangeo Platform; source: Abernathey et al (2017), “Pangeo: An Open Source Big Data Climate Science Platform “ NSF award 1740648.

6.2 Input parameters

All input parameters are set in one file in “.yaml” format. This format inherits from “json” one with more flexibility. The main advantages of the format are the human readability and natural reader/writer are provided as standard python libraries. The list of parameters are given below:

```
chronogram:
  N_macro_cycle : 15                # int : Number of macro-cycle for total simulation
  macro_cycle   : [12.,12.,12.,12.,12.] # Macro-cycle : list of incidences [deg]
  Npulse        : 1024              # Number of pulses per cycle
  cycle_duration:
    0.0 : 36.7e-3                  # Cycle duration of 0.0 deg incidence
    6.0 : 0.17                     # Cycle duration of 6.0 deg incidence
    12.0 : 0.17                    # Cycle duration of 12.0 deg incidence (36.7e-3 is no
  frequency     : 35.75e9           # Operational Electromagnetic frequency [Hz]
  polarization  : "VV"              # Operational polarisation ('VV', 'HH', 'VH', 'HV')
  slant_res     : 0.73              # 0.73 m => horizontal 3.5 m @ 12 degrees
  Ngates        : 3000              # Operational number of gates
```

```

sat_ground_speed : 7500.          # satellite ground speed [m/s]
altitude : 838e3                 # satellite altitude [m]
inclinaison : -98.              # Orbit inclination [deg]
bandwidth : 200e6               # Bandwidth [Hz]
pulse_length : 1e-6             # Pulse length [s]
PRF : 32e3                      # Pulse Repetition Frequency [Hz]
rotation_rate : 5.              # Antenna Rotation Rate in revolution per minute [r/m]
rotation : "clockwise"         # Rotation direction looking from above. Can be "clockwise" or "counterclockwise"
shift_sat_position: 0.          # Satellite position along the uptrack line at the beginning of the simulation [m]
shift_time: 0.                  # Initial time of the simulation [s]
shift_ant_azimuth: 90.         # Antenna azimuth relative to the uptrack direction [deg]
radial_aperture :
  0.0 : 0.57                    # Antenna radial aperture @ 0 degrees incidence [degree] (a)
  6.0 : 0.60                    # Antenna radial aperture @ 6 degrees incidence [degree] (a)
  12.0 : 0.66                   # Antenna radial aperture @ 12 degrees incidence [degree]
azimuthal_aperture :
  0.0 : 0.58                    # Antenna azimuthal aperture @ 0 degrees incidence [degree]
  6.0 : 0.60                    # Antenna azimuthal aperture @ 6 degrees incidence [degree]
  12.0 : 0.64                   # Antenna azimuthal aperture @ 12 degrees incidence [degree]

simulation:
output_directory : '/home1/datawork/fnouguie/research/output/RSSS' # Output directory
#~ output_filename : 'mysimulation.nc' # Output filename. Comment this line
#~ tmp_directory : '/home1/scratch/fnouguie/RSSS' # Tmp directory (should be a file)
numerical_sursampling_factor : 10 # Numerical sursampling factor
memory_divisor: 5 # Integer. Increase this factor if you have a lot of memory
flight_direction: 0. # Flight direction relative to North
#~ mss_s : 0.019 # Deprecated (automatically set to 0.019)
reference_pulse: 'middle' # Reference pulse of the cycle
# surface_filename : "SKIM_OS.nc" # temporary Surfaces name. This line is commented
#~ formatting: # If needed, Final formatting
#~ name : "kuros" # Formatting name
#~ integration_time : 1e-3 #additional parameter for formatting

surface:
size : [18000., 18000.] # size of the surface in [m, m]. Should be at least as large as the domain
dr : [1., 1.] # spatial sampling of the surface in [m, m].
dt : 0.07 # 0.07 time step at which surface is generated [s]
#~ spectrum_path: "/home1/datawork/fnouguie/research/ww3.OFFSHORE_201811_spec.nc" # WW3 spectrum
# spectrum_time_index: 0 # time index in WW3
# spectrum_station_index: 0 # station index in WW3
name : "elfouhaily" # name of wind sea spectrum (on-the-fly mode)
ws : 7. # wind speed [m/s] (on-the-fly mode)
wd : 90. # wind direction from North, clockwise. (on-the-fly mode)
cur : 1. # current velocity [m/s]. (on-the-fly mode)
curdir : -80. # current direction from North, clockwise. (on-the-fly mode)
directivity : "alongwind" # way the waves are moving ('alongwind', 'None'). (on-the-fly mode)
#~ omega : 0.84 # Inverse wave age (on-the-fly mode)
#~ sa : 2. # swell amplitude (can be a list) (on-the-fly mode)
#~ sd : -115. # swell direction (can be a list) from x direction (crosstrack), counterclockwise

```

```
#~ sk : 0.03          # swell wave number (can be a list).(on-the-fly mode)
#~ sp : None         # swell phase (on-the-fly mode)
#~ surface_path: "/home1/datawork/fnougue/research/output/ocean_surface/SKIM/SKIM_OS_wd=0_ws=7_dr="
```

```
cluster:
```

```
#~ cluster_configuration : "~/.config/dask/jobqueue.yaml"
```

6.3 Output files

For compatibility, all output files are in netCDF4 format.

6.4 Flow diagram

The Flow diagram can be divided in three steps:

- Initialization
- Main cycle iteration
- Formatting and finalization

6.5 Numerical code

Source code is freely available on <https://github.com/lanougue/RSSS>

A Appendix subsection

Bibliography

- Elfouhaily, T., B. Chapron, K. Katsaros, and D. Vandemark (1997). "A unified directional spectrum for long and short wind-driven waves". In: *J. Geophys. Res.* 102(C7), pp. 15781–15796.
- Mouche, A., D. Hauser, J.-F. Daloze, and C. Gu erin (2005). "Dual Polarisation Measurements at C-Band over the Ocean: Results from Airborne Radar Observations and Comparison with ENVISAT ASAR data". In: *IEEE Trans. on Geosci. and Remote Sensing* 43, pp. 753–769.
- Nouguier, F., A. Mouche, N. Rascle, B. Chapron, and D. Vandemark (2016). "Analysis of Dual-Frequency Ocean Backscatter Measurements at Ku- and Ka-Bands Using Near-Nadir Incidence GPM Radar Data". In: *IEEE Geoscience And Remote Sensing Letters* 31, pp. 2023–2245. DOI: 10.1109/LGRS.2016.2583198.
- Nouguier, F., B. Chapron, F. Collard, A. Mouche, N. Rascle, F. Ardhuin, and X. Wu (2018). "Sea surface kinematics from near-nadir radar measurements". In: *IEEE Trans. on Geosci. and Remote Sensing*. DOI: 10.1109/TGRS.2018.2833200. URL: http://tiny.cc/SKIMonRG_NOUG.

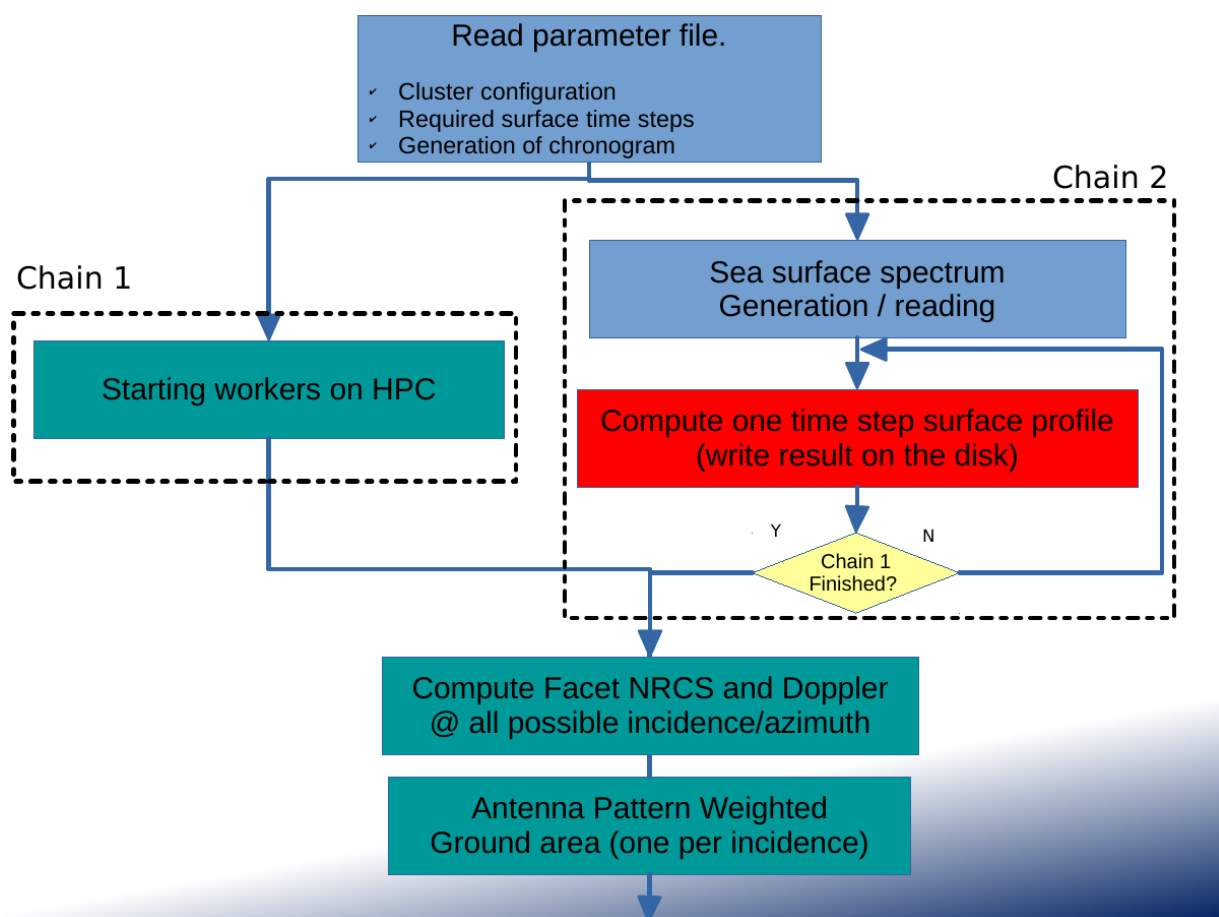


Figure 13: Initialization.

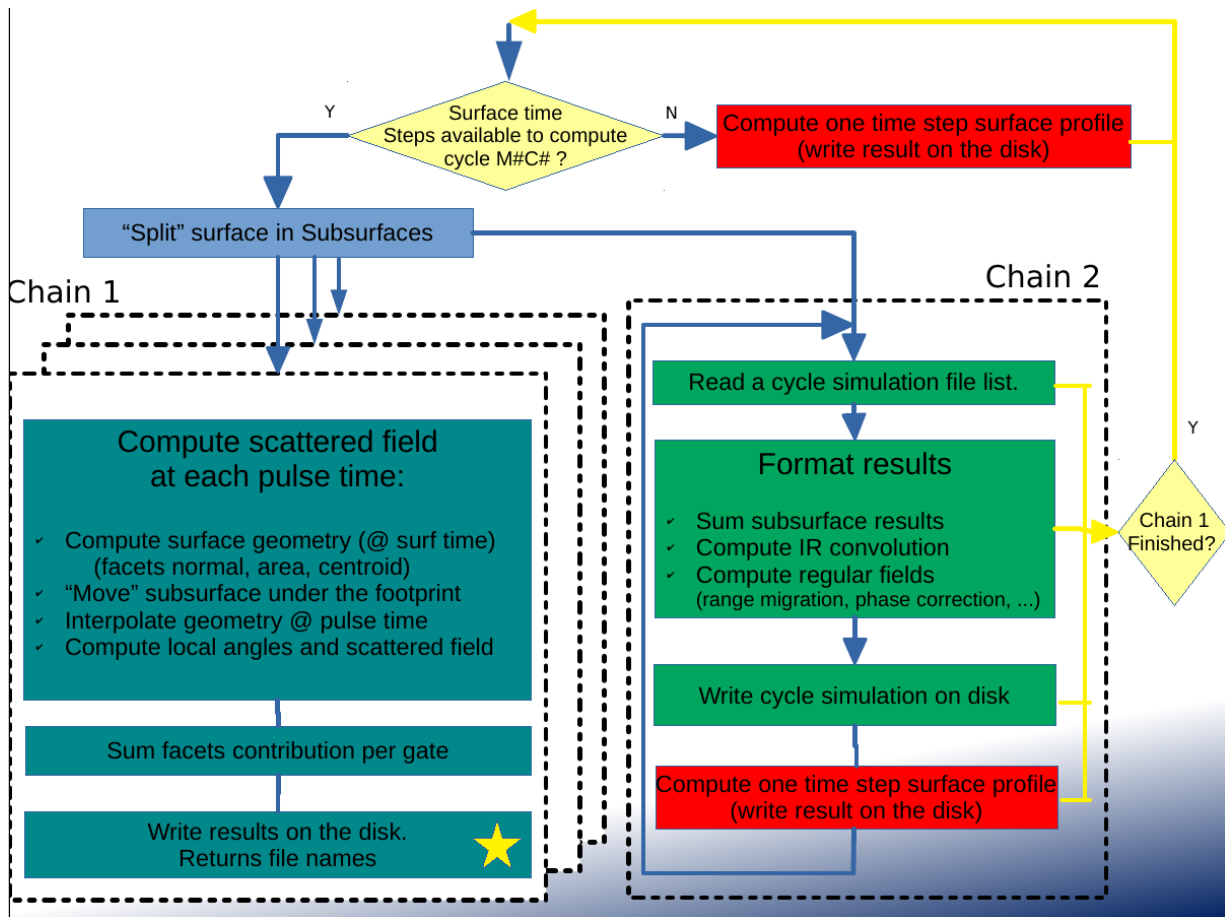


Figure 14: Main cycle iteration.

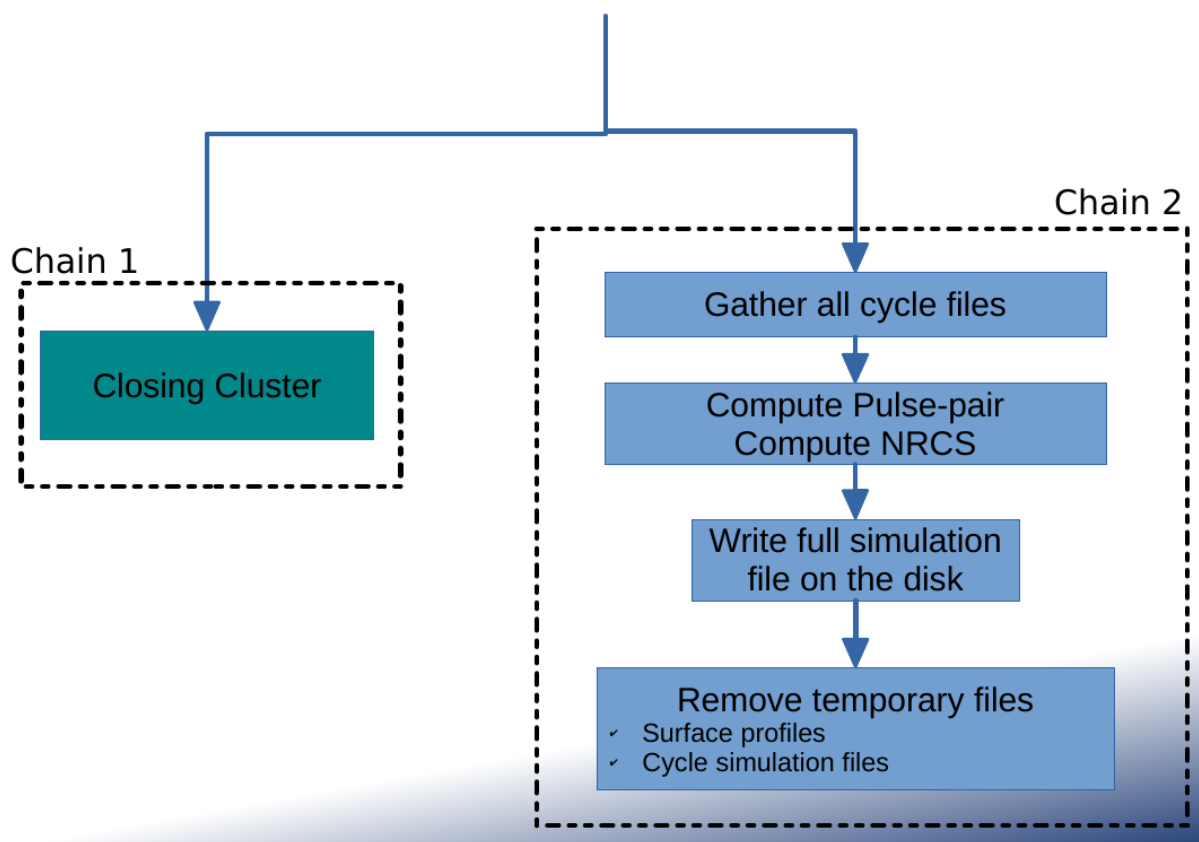


Figure 15: Finalization.